

Received XX Month, XXXX; revised XX Month, XXXX; accepted XX Month, XXXX; Date of publication XX Month, XXXX; date of current version XX Month, XXXX.

Digital Object Identifier 10.1109/XXXX.2025.1234567

Orthogonal Plane-Wave Transmit-Receive Isotropic-Focusing Micro-Ultrasound (OPTIMUS) with Bias-Switchable Row-Column Arrays

Darren Dahunsi¹, *Student Member, IEEE*, Randy Palamar¹, *Student Member, IEEE*, Tyler Henry¹, *Student Member, IEEE*, Mohammad Rahim Sobhani^{1,2}, *Student Member, IEEE*, Negar Majidi¹, *Student Member, IEEE*, Joy Wang¹, *Student Member, IEEE*, Afshin Kashani Ilkhechi^{1,2}, *Student Member, IEEE*, and Roger Zemp^{1,2}, *Member, IEEE*

¹Department of Electrical and Computer Engineering, University of Alberta, Edmonton, AB T6G 2R3, Canada

²CliniSonix Inc., Edmonton, AB T5J 4P6, Canada

Corresponding author: Darren Dahunsi (email: dahunsi@ualberta.ca).

RJZ and MRS are directors and shareholders of CliniSonix Inc., which provided partial support for this work. RJZ is a founder and director of OptoBiomeDx Inc., which, however, did not support this work. RJZ is also a founder and shareholder of IllumiSonics Inc., which, however, did not support this work. We gratefully acknowledge funding from the National Institutes of Health (R21HL161626-01 and EITTS/CA R21EY033078), Alberta Innovates (AICE 202102269, CASBE 212200391 and LevMax 232403439), MITACS (IT46044 and IT41795), CliniSonix Inc., NSERC (2025-05274) and a NSERC CGS-D to DD (588860 - 2024), the Alberta Cancer Foundation and the Mary Johnston Family Melanoma Grant (ACF JFMRP 27587), the Government of Alberta Cancer Research for Screening and Prevention Fund (CRSPPF 017061), an Innovation Catalyst Grant to MRS, INOVAIT (2023-6359), and an IBET Momentum Fellowship to DD. We are grateful to the nanoFAB staff at the University of Alberta for facilitating array fabrication.

ABSTRACT High quality structural volumetric imaging is a challenging goal to achieve with modern ultrasound transducers. Matrix probes have limited fields of view and element counts, whereas row-column arrays (RCAs) provide insufficient focusing. In contrast, Top-Orthogonal-to-Bottom-Electrode (TOBE) arrays, also known as bias-switchable RCAs can enable isotropic focusing on par with ideal matrix probes, with a field of view surpassing conventional RCAs. Orthogonal Plane-Wave Transmit-Receive Isotropic-Focusing Micro-Ultrasound (OPTIMUS) is a novel imaging scheme that can use TOBE arrays to achieve nearly isotropic focusing throughout an expansive volume. This approach extends upon a similar volumetric imaging scheme, Hadamard Encoded Row Column Ultrasonic Expansive Scanning (HERCULES), that is even able to image beyond the shadow of the aperture, much like typical 2D matrix probes. We simulate a grid of scatterers to evaluate how the resolution varies across the volume, and validate these simulations experimentally using a commercial calibration phantom. Experimental measurements were done with a custom fabricated TOBE array, custom biasing electronics, and a research ultrasound system. Finally we performed ex-vivo imaging to assess our ability to discern structural tissue information.

INDEX TERMS 3D imaging, hadamard encoded readout (HERO), hadamard encoded row column ultrasonic expansive scanning (HERCULES), orthogonal plane-wave transmit-receive isotropic-focusing micro-ultrasound (OPTIMUS), row-column arrays, top-orthogonal-to-bottom electrode (TOBE) arrays,

I. Introduction

VOLUMETRIC ultrasound imaging is an area of growing interest as transducer and computational capabilities increase and realtime volumetric imaging becomes more feasible. Newer transducer architectures such as matrix probes and row column arrays have potential to enable clin-

ical applications that require accurate 3-dimensional views of physiology. Volumetric views also better enable certain advanced imaging modes like elastography and blood flow imaging. Furthermore, 3D imaging may mitigate operator dependence. [1]–[7]

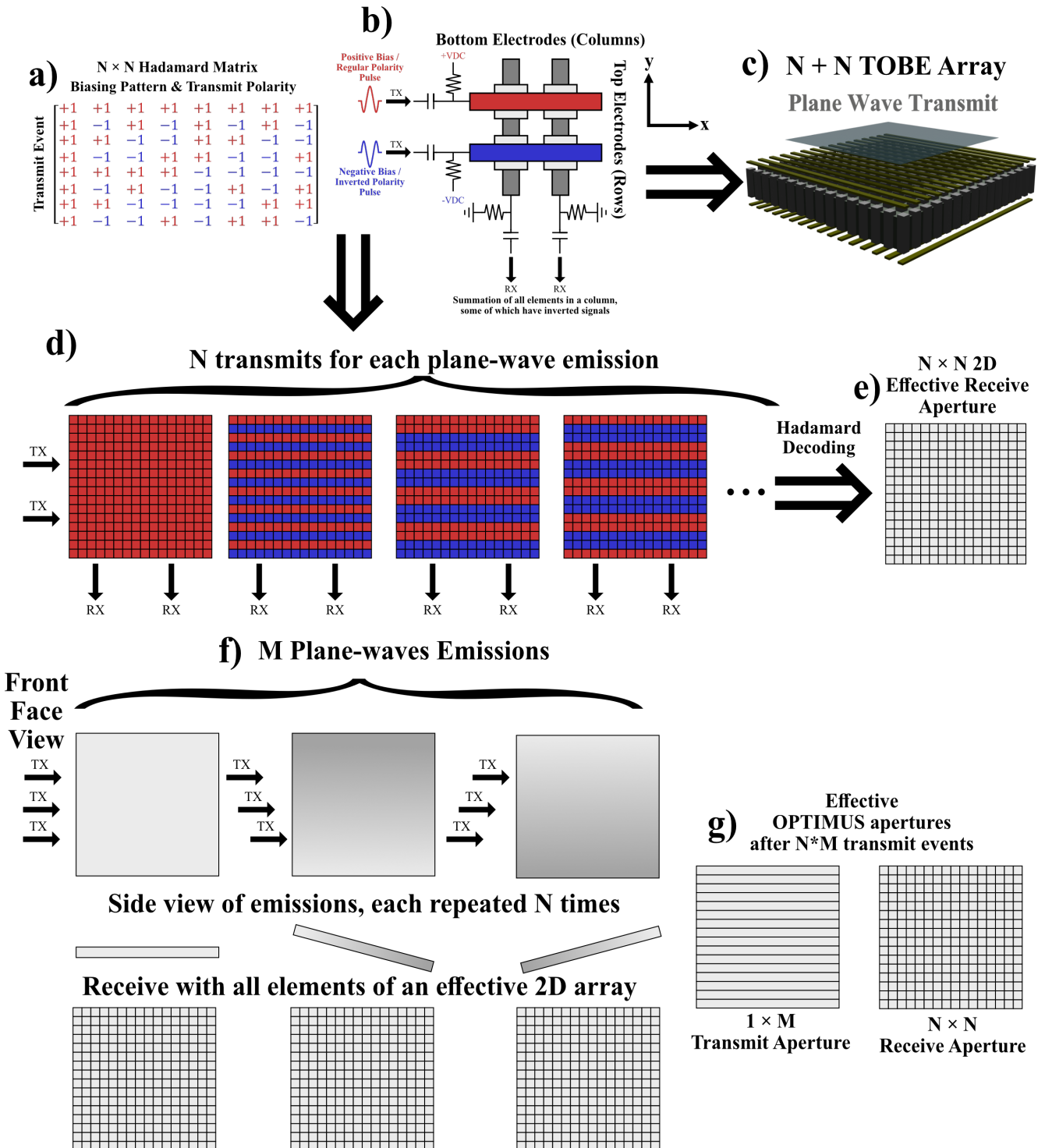


FIGURE 1: Summary of the OPTIMUS imaging scheme for an arbitrarily sized array of N rows and N columns with $N \times M$ transmit events. In a) we use the rows of a Hadamard matrix to determine the biasing and transmit polarities that are applied on the rows as shown in b), with each column of the matrix corresponding to a different row of the array. c) shows a render of the effective layout of the element electrodes on the transducer, and an effective transmit waveform. In d) we can see the effective bias pattern between each transmit event. For a set of N transmits the transmitted waveform will not change, but the received waveform will, and decoding will result in the receive aperture shown in e). f) We will repeat those N transmits for M different plane-wave angles and obtain the effective imaging aperture shown in g).

TABLE 1: Imaging Parameters

a) Transducer Parameters	Value
2D array size	128 + 128
Transmit Count	128
Pitch	250 μ m
Kerf	30 μ m
Center frequency	6.25 MHz
b) Simulation Parameters	Value
Number of excitation cycles	1
Speed of Sound	1540 m/s
Sampling frequency	50 MHz
c) Experimental Parameters	Value
Chirp Length	20e-6 μ s
Chirp Bandwidth	4–8 MHz
Speed of Sound	1452 m/s
Sampling frequency	16.6 MHz
d) Imaging Parameters	Value
Transmit Count (OPTIMUS)	1152
Transmit Count (HERCULES, VLS, TPW)	128
Angle Count (OPTIMUS)	9
Maximum Angle (OPTIMUS)	$\pm 10^\circ$
Maximum Angle (TPW)	$\pm 10^\circ$

Fully wired matrix probes have been proposed to achieve volumetric images, but the B-scan image quality is often inferior to clinical linear arrays which have a wide footprint and thus a low f-number. Scaling matrix probes up to similar footprints as these linear arrays is non-trivial. As the channel count of a 2D array increases quadratically, existing matrix probes are limited to small footprints, with 32×32 matrix probes being the largest commercial probes currently available. X-Matrix probes with microbeamformers require non-ideal beamforming approximations and wide beam transmits which negatively impact image quality. [1], [8]–[10]

Conversely, Row Column Arrays (RCAs) are able to have large footprints and large element counts, which promise high numerical apertures. However, because they are effectively two orthogonal linear arrays, they suffer from a lack of two-way focusing and are also constrained to imaging directly below the shadow of the aperture. There are previous RCA imaging schemes that use this architecture to perform volumetric imaging. Virtual line-source imaging (VLS) uses an array of virtual line sources as the transmit aperture, while Tilted Plane-Wave (TPW) imaging uses a series of tilted plane-waves [11]–[13]. Combined with using the orthogonal array as a receive aperture, RCAs can only perform one-way cylindrical focusing on transmit or receive, but not both. This is unlike an ideal fully-wired matrix probe that can perform two-way spherical focusing, and this limitation causes reduced image quality.

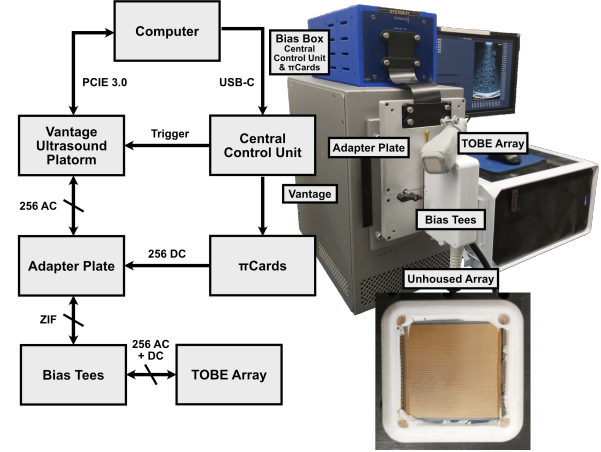


FIGURE 2: Setup for experimental imaging. We image with a Vantage Ultrasound Research platform, controlled by a host computer that also coordinates with the Central Control Unit of custom biasing electronics. The Central Control Unit controls the high-voltage biasing cards (π Cards), while waiting on triggers from the Vantage Unit to determine when to change the biasing pattern. The DC signals from the π Cards are mixed with AC signals from the Vantage and coupled on a bias tee and delivered to the TOBE array. An unhoused array is also shown.

Many modern volumetric imaging setups attempt to leverage the principles of ultrafast ultrasound imaging. Some of the primary benefits of ultrafast imaging are the decoupling of volume acquisition rate from volume resolution and the increased temporal coherence across the volume. On the other hand, insonifying the entire imaged region simultaneously reduces contrast [14]–[16]. Extended transmits like chirp excitations can be used to mitigate these types of issues, but in turn potentially introduce problems like a high mechanical index and probe heating [17]–[19]. Thankfully, the increased surface area of large specialized RCA arrays can mitigate these issues.

Electrostrictive top-orthogonal-to-bottom-electrode (TOBE) arrays are bias-sensitive RCAs that allow new capabilities beyond what conventional piezoelectric RCAs can enable. These electrostrictives are not inherently piezoelectric until a bias voltage is applied. This bias-sensitivity means that we can selectively enable sections of a transducer array. When this property is applied to a row-column array this allows us to manipulate or encode the effective aperture of the transducer on transmit or receive. By selectively activating parts of the array we can conduct full synthetic aperture imaging akin to a fully wired 2D array, however, due to the partial activation of the array, there is a significant decrease in SNR. Hadamard encoding presents a way to attain this fully wired capability without sacrificing signal strength.

In previous work we have shown that we can leverage hadamard encoding on bias-sensitive row column arrays to perform ultrafast imaging with a variety of imaging methods. In one method we perform transmit encoding and image 2D planes with high resolution by leveraging the large numerical aperture of our arrays [20]. This 2D imaging method is called Fast Orthogonal Row-Column Electronic Scanning (FORCES), and while it can create high quality images, it is limited to B-Mode imaging as there is no out-of-plane focusing. The B-Mode scan plane can be electronically steered, but constructing a volume at high resolution would take a very large amount of transmits. In another method we perform volumetric imaging with a receive aperture that mimics an ideal matrix probe, providing comparable volume quality to other existing RCA methods with the added benefit of being able to image beyond the shadow of the array [21]. This imaging method is called Hadamard Encoded Row-Column Ultrasonic Expansive Scanning (HERCULES), and it uses Hadamard encoding to create a virtual 2D receive aperture that can perform ideal spherical receive focusing. While HERCULES can make a volume at the same rate that FORCES can make a B-Mode slice, it is of lower quality, similar to other modern RCA imaging methods, due to HERCULES' lack of transmit focusing. This work introduces an iteration of HERCULES that can simultaneously provide transmit and receive focusing and obtain volumes with the quality of FORCES that have isotropic resolution. This imaging scheme is called Orthogonal Plane-Wave Transmit-Receive Isotropic-Focusing Micro-Ultrasound (OPTIMUS).

II. Methods

OPTIMUS relies on the use of the Hadamard-Encoded Read-Out (HERO) scheme to perform receive aperture encoding. This imaging method is described in full in [21], but we will give a brief description here.

We can model a row-column array of R rows and C columns as $R \times C$ 'physical elements'. The signal received at row r and column c for some emission pattern is $s_{rc}(t)$. Let's say we receive an ultrasound signal on the columns of an electrostrictive array held at DC ground while applying DC biases on the rows for E transmit events. If we construct a $R \times E$ matrix H from the bias of each row r for each transmit event e , we can express the signal received on column c for each transmit event e , $g_c^{\{e\}}(t)$ as:

$$g_c^{\{e\}}(t) = \sum_r H_r^{\{e\}} s_{rc}(t) \quad (1)$$

In matrix form, this is $\mathbf{g} = \mathbf{Hs}$, and thus we can create an estimate for the receive signal data $\hat{\mathbf{s}} = \mathbf{H}^{-1}\mathbf{g}$. A HERO acquisition is where we take H to be a $R \times R$ Hadamard matrix, and after $E = R$ transmit events we decode our channel data to obtain a signal dataset $\hat{s}_{rc}(t)$ that represents a virtual 2D receive aperture.

Performing a HERO acquisition will give us an effective receive aperture that matches a matrix array with full spher-

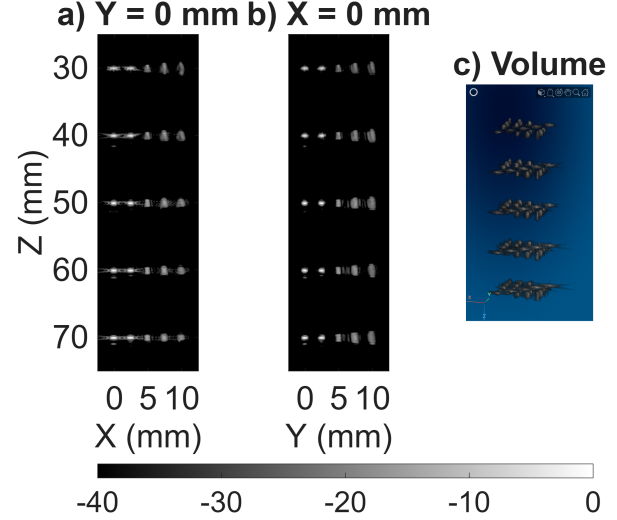


FIGURE 3: Simulations of a grid of point scatters imaged with OPTIMUS. a-b) are maximum intensity projections over a 5 mm slice, centered around a single plane of points in the XZ, YZ & XY planes, respectively. c) is a volume render of the 3D grid of scatters.

ical focusing. However, our transmit aperture is completely unfocused. To provide transmit focusing OPTIMUS will repeatedly perform HERO acquisitions with varying transmit delay profiles. As we are still using a row column array, this will only provide cylindrical transmit focusing, but combined with full spherical receive focusing this provides near isotropic resolution. Figure 1 shows a summary of this imaging scheme.

A. Simulation

To assess the isotropy of OPTIMUS we simulated a field of scatterers using FieldII. Scatterers are placed at various positions in the transducer's field of view and we measure the point spread function profiles and how they vary across space. Table 1 a), b) & d) lists the simulation parameters.

B. Experiment

We used a custom-fabricated 4-8 MHz 128×128 TOBE array (CliniSonix, Edmonton, AB, Canada) [22], [23] to implement OPTIMUS and image various commercial phantoms and ex-vivo samples. We used custom biasing electronics connected to a Vantage 256 High Frequency Ultrasound System (Verasonics, Kirkland, WA, USA) [24]. We couple DC signals from the biasing electronics and AC signals from the Vantage to drive the transducer. Figure 2 shows the experimental setup, and Table 1 a), c) & d) lists the experimental properties.

We imaged a commercial quality assurance phantom (ATS 539, CIRS Inc., Norfolk, VA, USA) to characterize the quality of our imaging scheme. We compared OPTIMUS with other volumetric imaging techniques such as HERCULES, Virtual Line Source (VLS), & Tilted Plane-Wave Imaging

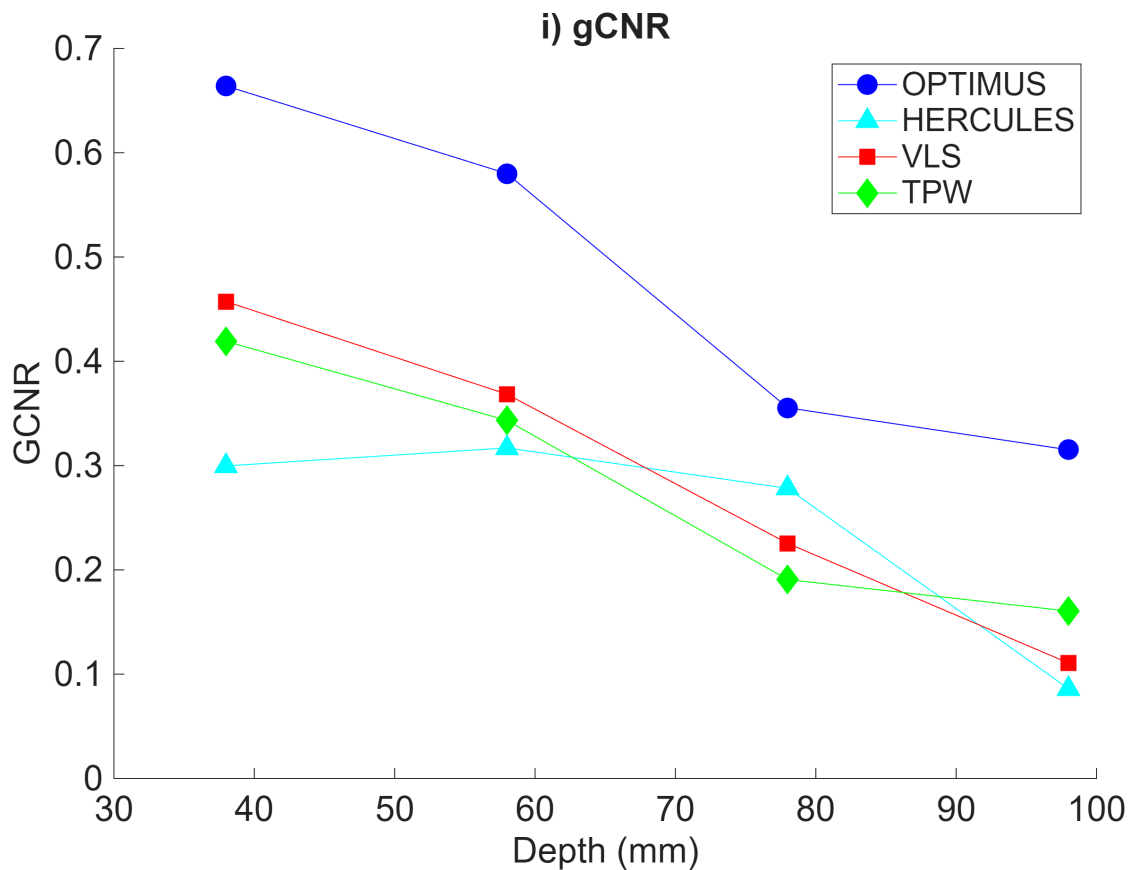
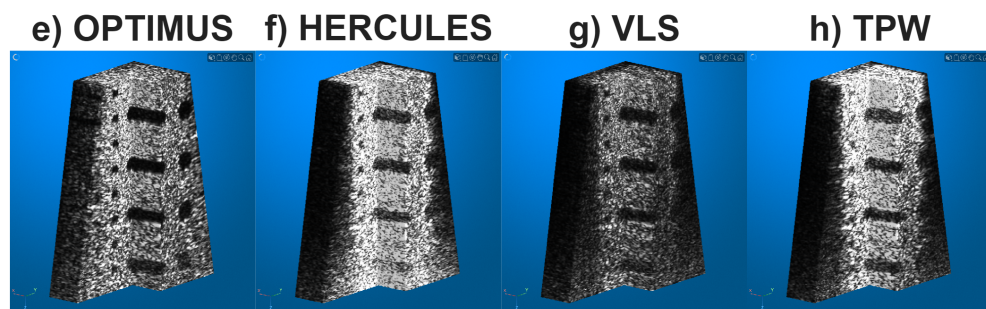
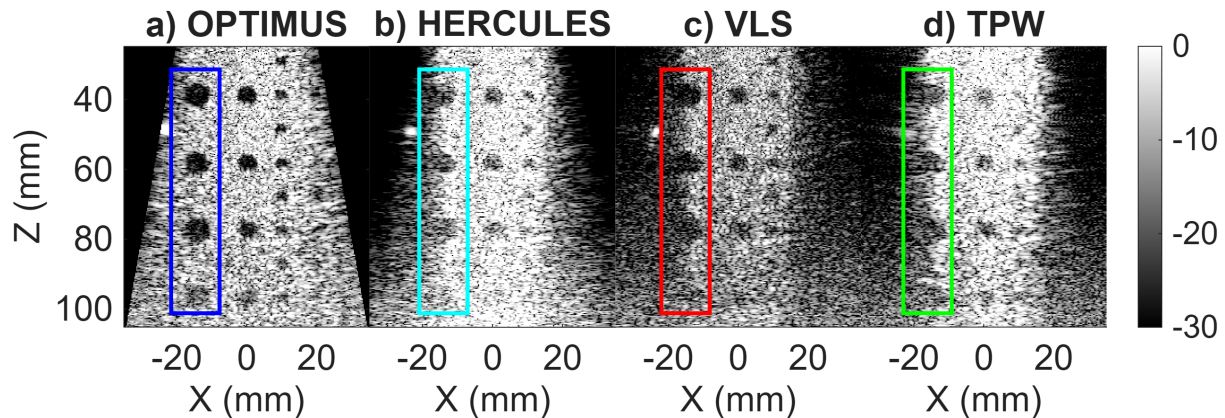


FIGURE 4: Experimental volume imaging of a commercial calibration phantom (CIRS ATS 539). a-d) show the center slice of the volumes, and e-h) show cut-outs. i) is a measurement of the gCNR of the largest cysts. The HERCULES, VLS & TPW volumes were created using 128 emissions, while the OPTIMUS volume was created using 1152 emissions.

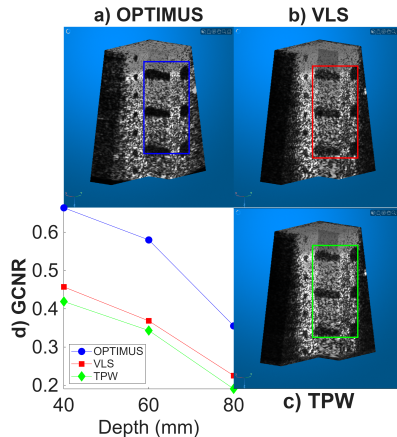


FIGURE 5: Experimental comparisons of OPTIMUS with standard RCA imaging methods using an equal number of emissions. All 3 volume were created using 1152 emissions. The gCNR of the largest cysts are plotted in d).

[21], [25], [26]. We also imaged an ex-vivo pig fetus to demonstrate real tissue imaging capabilities. The fetus was immersed in a water bath for coupling. This imaging was performed using chirp excitations to compensate for reduced SNR caused by unfocused insonification.

C. Processing

After receiving data from the Vantage system, we apply a matched filter and demodulate our signal to baseband. For our encoded imaging schemes, HERCULES & OPTIMUS, we need to perform a decoding step, where we use the inverse of the Hadamard matrix H to recover s_{rc} . This provides us with the dataset of a virtual 2D receive aperture. At this point we can apply standard synthetic aperture delay-and-sum beamforming and obtain a volume.

TABLE 2: Scatter Grid Resolutions

Metric	Normalized (μm per $\lambda f\#$)
Lateral Resolution	1.60 ± 0.46
Elevational Resolution	1.42 ± 0.39
Metric	Normalized (μm per $\lambda f\#$)
Axial Resolution	2.76 ± 1.91

III. Results

Figure 3 displays some sample point-spread-functions (PSFs) from our scatterer grid simulation. In Table 2 we plot resolution metrics as they vary across the medium. The average lateral and elevational resolution match the theoretical lateral resolution of $\text{FWHM} = 1.4F\# = 1.4 * f/D$ where FWHM is the full-width-half-maximum value of the profile, $F\#$ is the f-number which is equivalent to the ratio of the focal length f and the characteristic length of the aperture D . The lateral and elevational resolution does increase as points

go deeper, but that is expected as the $F\#$ increases. The variation as x or y changes is relatively small. The axial resolution increases in variance away from the central axis of the transducer, potentially decreasing fidelity at the edges of the volume. Typical 3D imaging schemes using 2D arrays have PSFs that vary significantly across the array's field of view, but OPTIMUS is able to maintain relative consistency, nearly up to the edge of the shadow of the aperture.

Experimental characterization of OPTIMUS is shown in our phantom images in Figure 4. It is compared with HERCULES, VLS, & TPW. HERCULES, VLS & TPW all show comparable results, but VLS & TPW are unable to image beyond the shadow of the aperture. All three methods show ideal resolution along the receive direction, but display quality degradation in the transmitting direction. In contrast, OPTIMUS does not display any difference in the transmit direction. The figure also shows a quantitative comparison of the imaging method's contrast. OPTIMUS displays significantly higher gCNR than any of the other imaging methods. Videos of other imaging phantoms imaged with OPTIMUS are provided in the supplementary material.

To evaluate whether OPTIMUS' performance is purely a product of increased SNR due to a higher transmit count, we compared OPTIMUS to VLS & TPW acquisitions consisting of an equal number of transmits. Figure 5 shows both visual and quantitative comparisons. The marginal improvements of VLS & TPW diminish as the transmit count increases, and they are unable to achieve the same level of quality that OPTIMUS can. In a clinical scenario where this extended acquisition is not problematic, OPTIMUS provides significant advantages.

Figure 6 demonstrates in-vivo imaging of a fetal pig with OPTIMUS. Volume flythroughs are provided in the supplementary material. In these volumes we can distinguish organs in various portions of the body. The large footprint of our array coupled with the wide FOV of OPTIMUS allow us to image a large portion of the fetus.

The main drawback of an OPTIMUS acquisition is the transmit count. The volumes in the previous figures are acquired at 9 angles, and when combined with decoding on a 128×128 array requires 1152 transmit-receive events. At a 10 KHz base PRF we are limited to a 8.7Hz acquisition rate. This is sufficient for ex-vivo imaging, but potentially prohibitive for clinical applications where large motion is expected. However, these problems can potentially be mitigated with motion compensation between lower resolution volumes. These low resolution volumes could be acquired by using 128 emissions at a single angle, but a partial decoding technique could be used to reduce the required emissions to as few as 16 [27].

IV. Conclusion

In this work we demonstrated a new imaging method that performs high quality isotropic volumetric imaging using the properties of bias-sensitive row column arrays. This

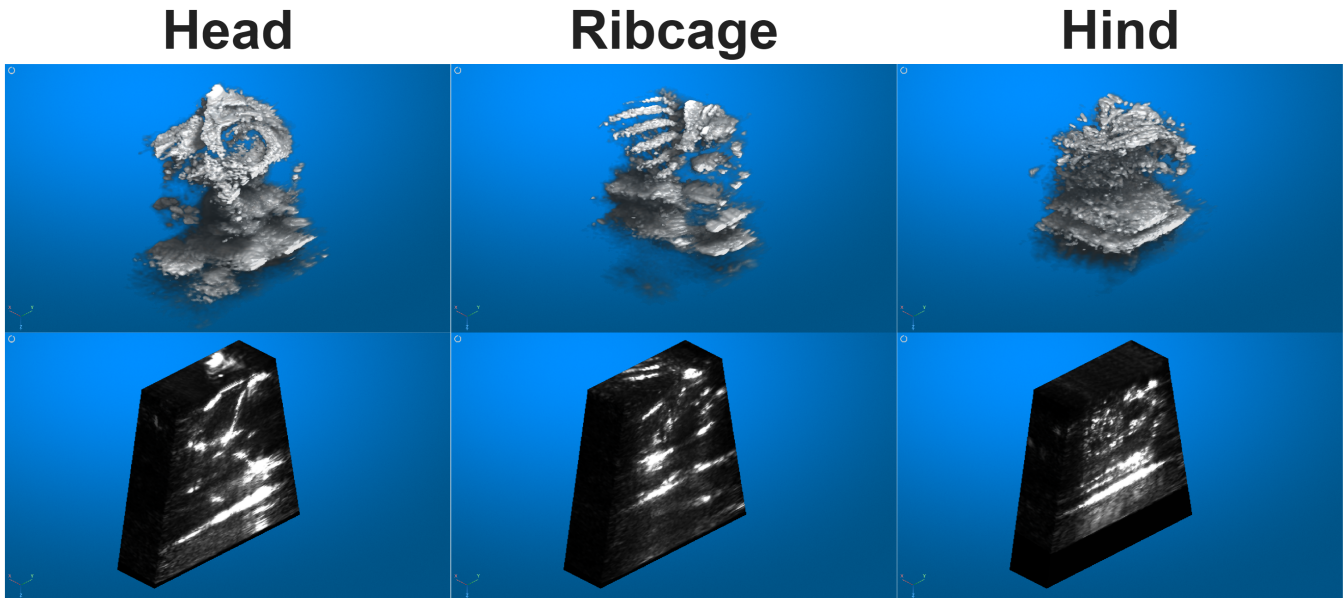


FIGURE 6: Ex-vivo Fetal Pig. Fetus was imaged while immersed in a water bath to maximize coupling with the transducers. Using OPTIMUS we generated expansive volumes of the fetus at it's head, ribcage and hind legs. A maximum intensity projection is shown on the top figures, while a cut plane at center of the volumes is shown on the bottom. Videos are provided in the supplementary materials.

method has superior resolution and contrast to other existing volumetric imaging methods, at the cost of a slow acquisition rate. This makes it a good candidate for imaging static features and generating structural images, such as visualizing the margins of an excised tumor. Motion compensation can be leveraged to mitigate the negative effects of compounding. Future work could include using an array with an acoustic lens to acquire full pyramidal volumes, or applying computer vision techniques to perform automatic segmentation of tissue structures in realtime.

REFERENCES

[1] S. Smith, H. Pavly, and O. von Ramm, "High-speed ultrasound volumetric imaging system. i. transducer design and beam steering," *IEEE Transactions on Ultrasonics, Ferroelectrics, and Frequency Control*, vol. 38, no. 2, pp. 100–108, 1991.

[2] J. N. Welch, J. A. Johnson, M. R. Bax, R. B. M.D., S. S. M.D., T. Krummel, and R. Shahidi, "Real-time freehand 3D ultrasound system for clinical applications," in *Medical Imaging 2001: Visualization, Display, and Image-Guided Procedures*, S. K. Mun, Ed., vol. 4319, International Society for Optics and Photonics. SPIE, 2001, pp. 724 – 730. [Online]. Available: <https://doi.org/10.1117/12.428120>

[3] A. Austeng and S. Holm, "Sparse 2-d arrays for 3-d phased array imaging design methods," *IEEE Transactions on Ultrasonics, Ferroelectrics, and Frequency Control*, vol. 49, no. 8, pp. 1073–1086, 2002.

[4] J. Yen and S. Smith, "Real-time rectilinear 3-d ultrasound using receive mode multiplexing," *IEEE Transactions on Ultrasonics, Ferroelectrics, and Frequency Control*, vol. 51, no. 2, pp. 216–226, 2004.

[5] H. Chang, Z. Chen, Q. Huang, J. Shi, and X. Li, "Graph-based learning for segmentation of 3d ultrasound images," *Neurocomputing*, vol. 151, pp. 632–644, 2015. [Online]. Available: <https://www.sciencedirect.com/science/article/pii/S0925231214013873>

[6] D. B. Downey and A. Fenster, "Vascular imaging with a three-dimensional power doppler system," *American Journal of Roentgenology*, vol. 165, no. 3, pp. 665–668, 1995, pMID: 7645492. [Online]. Available: <https://doi.org/10.2214/ajr.165.3.7645492>

[7] Q. Huang, B. Xie, P. Ye, and Z. Chen, "Correspondence 3-d ultrasonic strain imaging based on a linear scanning system," *IEEE Transactions on Ultrasonics, Ferroelectrics, and Frequency Control*, vol. 62, no. 2, pp. 392–400, 2015.

[8] O. von Ramm, S. Smith, and H. Pavly, "High-speed ultrasound volumetric imaging system. ii. parallel processing and image display," *IEEE Transactions on Ultrasonics, Ferroelectrics, and Frequency Control*, vol. 38, no. 2, pp. 109–115, 1991.

[9] B. Heiles, M. Correia, V. Hingot, M. Pernot, J. Provost, M. Tanter, and O. Couture, "Ultrafast 3d ultrasound localization microscopy using a 32×32 matrix array," *IEEE Transactions on Medical Imaging*, vol. 38, no. 9, pp. 2005–2015, 2019.

[10] J. Zhang, D. Wang, J. An, F. Dong, F. Feng, J. Yin, S. Huang, W. Guo, and J. Zhang, "3d contrast-enhanced ultrasound imaging of the muscle using a sparsely controlled matrix array probe," in *2021 IEEE International Ultrasonics Symposium (IUS)*, 2021, pp. 1–4.

[11] S. I. Awad and J. T. Yen, "3-d spatial compounding using a row-column array," *Ultrasonic Imaging*, vol. 31, no. 1, pp. 120–130, 2009, pMID: 19630253. [Online]. Available: <https://doi.org/10.1177/016173460903100103>

[12] M. Flesch, M. Pernot, J. Provost, G. Ferin, A. Nguyen-Dinh, M. Tanter, and T. Deffieux, "4d in vivo ultrafast ultrasound imaging using a row-column addressed matrix and coherently-compounded orthogonal plane waves," *Physics in Medicine & Biology*, vol. 62, no. 11, p. 4571, may 2017. [Online]. Available: <https://dx.doi.org/10.1088/1361-6560/aa63d9>

[13] L. T. Jørgensen, S. K. Praesius, M. B. Stuart, and J. A. Jensen, "Row-column beamformer for fast volumetric imaging," *IEEE Transactions on Ultrasonics, Ferroelectrics, and Frequency Control*, vol. 70, no. 7, pp. 668–680, 2023.

[14] G. Montaldo, M. Tanter, J. Bercoff, N. Benech, and M. Fink, "Coherent plane-wave compounding for very high frame rate ultrasonography and transient elastography," *IEEE Transactions on Ultrasonics, Ferroelectrics, and Frequency Control*, vol. 56, no. 3, pp. 489–506, 2009.

[15] M. Couade, M. Pernot, M. Tanter, E. Messas, A. Bel, M. Ba, A.-A. Hagège, and M. Fink, "Ultrafast imaging of the heart using circular wave synthetic imaging with phased arrays," in *2009 IEEE International Ultrasonics Symposium*, 2009, pp. 515–518.

[16] M. Tanter and M. Fink, "Ultrafast imaging in biomedical ultrasound," *IEEE Transactions on Ultrasonics, Ferroelectrics, and Frequency Control*, vol. 61, no. 1, pp. 102–119, 2014.

[17] C. Kollmann, G. Vacariu, V. Fialka-Moser, and H. Bergmann, "Measuring the surface-heating of medical ultrasonic probes," *Journal of Physics: Conference Series*, vol. 1, no. 1, p. 78, jan 2004. [Online]. Available: <https://doi.org/10.1088/1742-6596/1/1/018>

[18] J. Calvert, F. Duck, S. Clift, and H. Azaime, "Surface heating by transvaginal transducers," *Ultrasound in Obstetrics & Gynecology*, vol. 29, no. 4, pp. 427–432, 2007. [Online]. Available: <https://obgyn.onlinelibrary.wiley.com/doi/abs/10.1002/uog.3973>

[19] A. Nowicki, "Safety of ultrasonic examinations; thermal and mechanical indices," *Medical Ultrasonography*, vol. 22, no. 2, pp. 203–210, 2020. [Online]. Available: <https://www.medultrason.ro/medultrason/index.php/medultrason/article/view/2372>

[20] C. Ceroici, T. Harrison, and R. J. Zemp, "Fast orthogonal row-column electronic scanning with top-orthogonal-to-bottom electrode arrays," *IEEE Transactions on Ultrasonics, Ferroelectrics, and Frequency Control*, vol. 64, no. 6, pp. 1009–1014, 2017.

[21] D. O. Dahunsi, R. Palmar, T. Henry, M. R. Sobhani, N. Majidi, J. Wang, A. K. Ilkhechi, J. Brown, and R. Zemp, "Hadamard encoded row column ultrasonic expansive scanning (hercules) with bias-switchable row-column arrays," 2025. [Online]. Available: <https://arxiv.org/abs/2506.11443>

[22] A. Sampaleanu, P. Zhang, A. Kshirsagar, W. Moussa, and R. J. Zemp, "Top-orthogonal-to-bottom-electrode (tobe) cmut arrays for 3-d ultrasound imaging," *IEEE Transactions on Ultrasonics, Ferroelectrics, and Frequency Control*, vol. 61, no. 2, pp. 266–276, 2014.

[23] R. K. Chee, A. Sampaleanu, D. Rishi, and R. J. Zemp, "Top orthogonal to bottom electrode (tobe) 2-d cmut arrays for 3-d photoacoustic imaging," *IEEE Transactions on Ultrasonics, Ferroelectrics, and Frequency Control*, vol. 61, no. 8, pp. 1393–1395, 2014.

[24] A. K. Ilkhechi, R. Palamar, M. R. Sobhani, D. Dahunsi, C. Ceroici, M. Ghavami, J. Brown, and R. Zemp, "High-voltage bias-switching electronics for volumetric imaging using electrostrictive row–column arrays," *IEEE Transactions on Ultrasonics, Ferroelectrics, and Frequency Control*, vol. 70, no. 4, pp. 324–335, 2023.

[25] M. F. Rasmussen, T. L. Christiansen, E. V. Thomsen, and J. A. Jensen, "3-d imaging using row-column-addressed arrays with integrated apodization - part i: apodization design and line element beamforming," *IEEE Transactions on Ultrasonics, Ferroelectrics, and Frequency Control*, vol. 62, no. 5, pp. 947–958, 2015.

[26] K. Chen, B. C. Lee, K. E. Thomenius, B. T. Khuri-Yakub, H.-S. Lee, and C. G. Sodini, "A column-row-parallel ultrasound imaging architecture for 3-d plane-wave imaging and tx second-order harmonic distortion reduction," *IEEE Transactions on Ultrasonics, Ferroelectrics, and Frequency Control*, vol. 65, no. 5, pp. 828–843, 2018.

[27] T. K. Henry, D. Dahunsi, R. Palamar, N. Majidi, M. R. Sobhani, A. K. Ilkhechi, and R. Zemp, "Recursive aperture decoded ultrasound imaging (READI) with estimated motion-compensated compounding (EMC2)," 2025. [Online]. Available: <https://arxiv.org/abs/2509.08781>